PointVS: A Machine Learning Scoring Function that Identifies Important Binding Interactions

Jack Scantlebury[1,*], **Lucy Vost**[1,*], **Anna Carbery**[1,2], **Thomas E. Hadfield**[1], **Oliver M. Turnbull**[1], **Nathan Brown**[3], **Vijil Chenthamarakshan**[4], **Payel Das**[4], **Harold Grosjean**[5], **Frank von Delft**[2,6,7,8], and **Charlotte M. Deane**[1,**]

[1] *Department of Statistics, University of Oxford, Oxford, UK*

[2] *Diamond Light Source Ltd., Harwell Science and Innovation Campus, Didcot, UK*

[3] *Healx, Charter House, Cambridge, UK; at time of work: BenevolentAI, London, UK*

[4] *IBM Thomas J. Watson Research Center, New York, USA*

[5] *Structural Genomics Consortium, University of Oxford, Oxford, UK*

[6] *Centre for Medicines Discovery, University of Oxford, Oxford, UK*

[7] *Department of Biochemistry, University of Johannesburg, Johannesburg, South Africa*

[8] *Research Complex at Harwell, Harwell Science and Innovation Campus, Didcot, UK*

[*] *Authors contributed equally*

[**] *deane@stats.ox.ac.uk*

ABSTRACT

Over the last few years, many new machine learning-based scoring functions for predicting the binding of small molecules to proteins have been developed. Their objective is to approximate the distribution which takes two molecules as input and outputs the energy of their interaction. This distribution is dependent on the interatomic interactions involved in binding, and only a scoring function that accounts for these interactions can accurately predict binding affinity on unseen molecules. To try to create a method capable of learning these interactions, we built PointVS: a machine learning-based scoring function which achieves state of the art performance even after rigorous filtering of the training set. This filtering is key, as we found that a commonly used benchmark, CASF-16, overestimates the true accuracy of machine learning-based scoring functions when trained using the most commonly used training set. Ranking algorithms using this benchmark rewards memorisation of training data rather than knowledge of the rules of intermolecular binding. We demonstrate that PointVS is able to identify important interactions using attribution, and further, that it can be used to extract important binding pharmacophores from a given protein target when supplied with a number of bound structures. We use this information to perform fragment elaboration, and see improvements in docking scores compared to using structural information from a traditional data-based approach. This not only provides definitive proof that PointVS is learning to identify important binding interactions, but also constitutes the first deep learning-based method for extracting structural information from a target for molecule design.

1. Introduction

Drug design aims to optimise molecules to achieve a desired biological response. Typically led by human experts, this process is time-consuming and expensive, with recent estimates placing the time required to reach clinical trials at 8.3 years, and the median cost at $985 million.[1] Computational techniques offer a promising alternate route to human-led design.

One such computational technique is docking.[2,3] Docking algorithms take as input the coordinates of protein and ligand atoms, and predict the possible conformations of the protein-ligand complex. There exists a function describing the energy of the complex, and as conformational space is searched, this function is minimised. In the case of a deterministic algorithm with a single starting conformation, a single output pose is generated along with an estimation of the binding affinity; for a probabilistic search, or any search with multiple starting conformations, the result is a list of binding poses. These are ranked in the order of estimated binding affinity. Affinities are calculated using a scoring function, which uses a combination of atomic interactions to approximate the binding energy.

Over the last decade, machine learning models have shown promise in predicting both the pose and energetics of protein-ligand binding.[4,5] In particular, deep learning mod-

els, which can be made to approximate extremely complex functions,[6] have been used to predict binding affinities as well as designing *de novo* molecules satisfying a variety of constraints.[7,8] The binding affinity of a given molecule to a protein target is a function of the positions and identities of its atoms, which can be approximated by a neural network in a machine learning-based scoring function (MLBSF). Given the coordinates of a protein-ligand complex (obtained by docking or otherwise), such a function considers all interactions between the two molecules. In this way, the interaction energies between two unseen molecules could be predicted.

Recent research into MLBSFs has highlighted their tendency to learn dataset biases, rather than physical interactions.[9–12] In these cases, the MLBSFs perform less of an assessment of atomic contributions, and something more analogous to a nearest-neighbours search in ligand-pocket space. This is useful if the application is to proteins or scaffolds with a large amount of previous binding data available, but not for new targets or ligands, as the true functional relationship governing binding is not learned. This problem is often exacerbated by a lack of rigorous dataset filtering. One of the most widely used benchmarks for scoring functions, both classical and machine learning-based, is the Comparative Assessment of Scoring Functions, 2016 (CASF-2016).[13] The usual method of training a MLBSF is to train on the PDBBind[14] general set of crystal structures and binding affinities after removing the structures in CASF-2016. As we show in this paper, this approach suffers from information leakage concerning almost every test structure, resulting in an overestimation of the accuracy of MLBSFs.

There is an active area of research surrounding how machine learning models make predictions,[15–18] a technique known as input attribution. Such techniques can be applied to MLBSFs; the idea being that an ideal MLBSF—one which has learnt to distinguish atomic interactions, rather than just dataset biases—should be able to identify the most important binding interactions for a given protein target.

This binding information could then be leveraged in other stages of the drug development pipeline. In practice, attribution analyses depend on the architecture of the MLBSF. The two prevalent deep learning architectures used as scoring functions are convolutional neural networks (CNNs)[19–21] and graph neural networks (GNNs).[22,23] Attribution for CNN-MLBSFs is limited, because spatial relationships are lost as information flows deeper into the network.[24] GNNs, on the other hand, preserve the concept of the atom until the final layers of the network, so atom embeddings and edges can be interrogated for information.

Input attribution on MLBSFs is a promising approach for extracting binding insights from a protein, for example, for fragment-based drug discovery (FBDD); a strategy that seeks to identify simple, small molecules (fragments) that interact with protein targets, and grow them into active leads. In order to meaningfully add atoms to these molecules, structural knowledge about the target needs to be considered. This can be extracted from known binders, but this limits the exploration of chemical space as well as restricting the applicability of the approach to targets with known ligands. Extracting structural information directly from the protein itself is therefore advantageous. Currently, there is only one available generative model for fragment elaboration that relies solely on protein structure.[25] This method uses a data-driven approach[26] to identify 'hotspots': regions in the protein pocket that contribute disproportionately to binding. Currently there exists no deep learning-based tool to identify such regions.

Here we present PointVS, a group-invariant GNN. It is a MLBSF designed to predict both binding affinity and pose score. We show that it achieves competitive performance on the CASF-2016 benchmark—even after rigorously filtering the training dataset to avoid training on proteins or ligands similar to test structures—hence demonstrating its ability to learn spatial information. We then use attribution to show that the model successfully identifies important binding interactions, and further, that this information can be leveraged to perform fragment elaboration resulting in improved docking scores compared to using a data-driven approach. We make our code as well as our unbiased test and train splits available on GitHub at github.com/oxpig/PointVS.

2. Methods

An overall schema of the methods used to debias and test PointVS is shown in Fig 1.

2.1 Model

A graph is a natural way of representing a molecule, and attribution to individual inputs—namely atoms—is an intuitive process when using graph neural networks (GNNs). We use an architecture based on *E(n)*-Equivariant Graph Neural Network (EGNN) layers.[27] The $E(n)$ symmetry group contains all elements from $SE(n)$, as well as the group of all reflections; EGNN layers are also permutation-equivariant, meaning that the network is invariant to the order of the input vertices.

PointVS is a lightweight $E(n)$-equivariant graph neural network layer model, consisting of an initial projection to take the number of node features from 12 to 32, then 48 EGNN

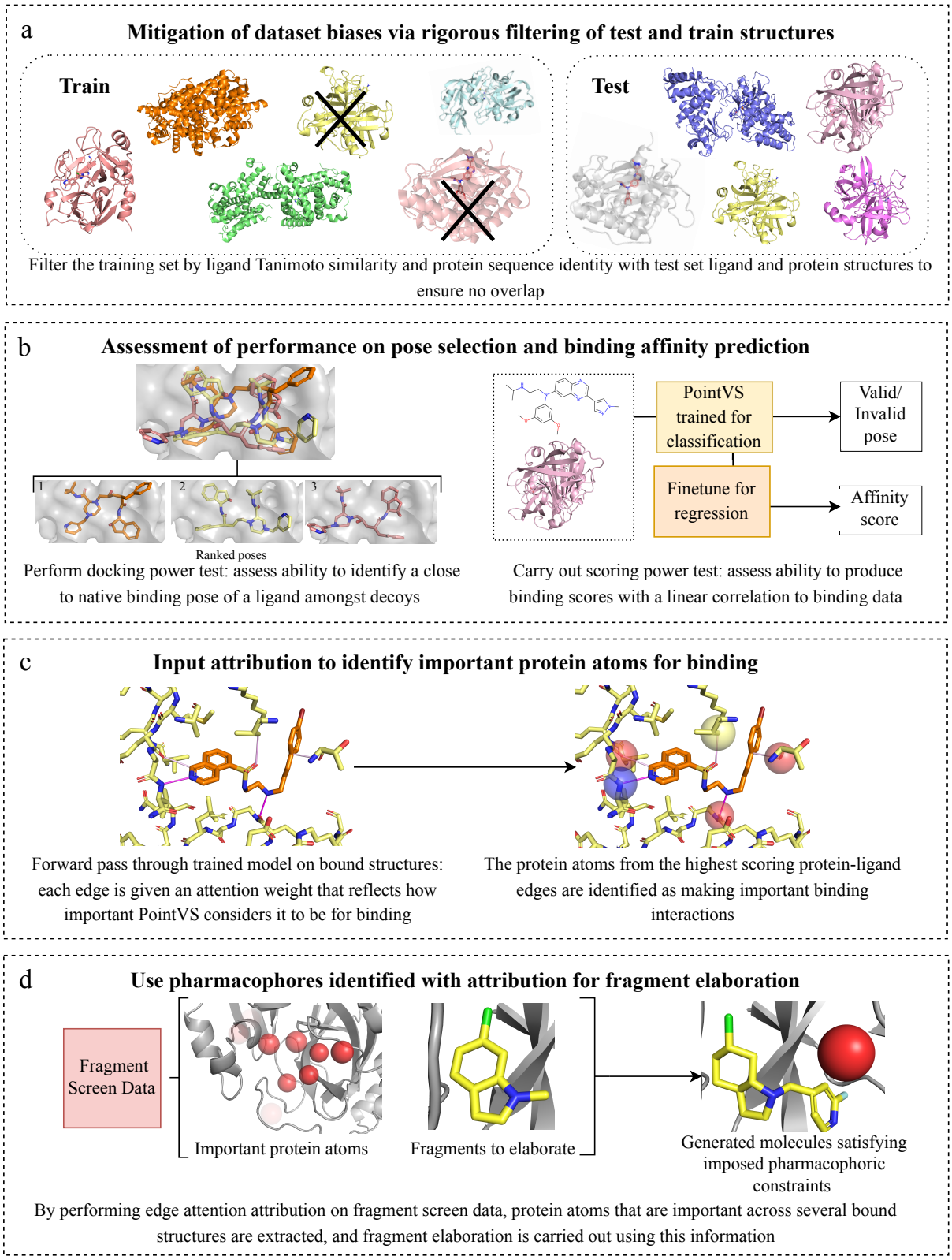

Fig. 1. An overall schema of the methods used to debias and test PointVS. We first thoroughly filter the test and train sets (box a), before benchmarking the performance of PointVS on the docking power and scoring power tests (b). We then use attribution to gain insights into important binding regions in the protein pocket (c), which we use for fragment elaboration (d).

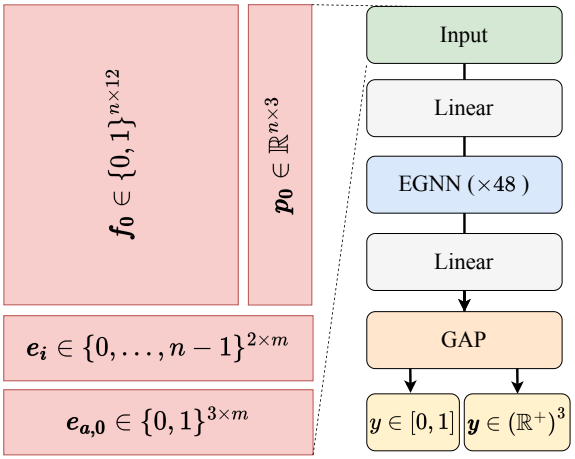

Fig. 2. Architecture and input format of PointVS. Each of the n atoms in the input to the model (left) is given a one-hot encoded feature vector with a single bit added to indicate whether the atom is from the ligand or the receptor, as well as a position $\boldsymbol{p_0} \in \mathbb{R}^3$. There are m edges, defined by the edge indices $\boldsymbol{e_i} \in \{0,...,n-1\}^{2\times m}$ which are the indices of connected atoms, and the corresponding edge attributes $\boldsymbol{e_a} \in \{0,1\}^{3\times m}$. These are one-hot encodings representing ligand-ligand, ligand-protein, and protein-protein edges. There are skip connections between each of the EGNN layers, and the linear and global average final pooling (GAP) layers only act upon the node features f.

layers, followed by a global average pooling of the final node embeddings. This is followed by a sigmoid layer which gives a label $y \in [0,1]$ during the first stage of training on pose prediction. During finetuning on affinity data, this final layer is replaced by an randomly initiated fully connected layer and ReLU activation, which outputs $\mathbf{y} \in (\mathbb{R}^+)^3$ (see Fig 2). This architecture includes residual connections for node features to allow for easier gradient flow and a richer combination of early and late representations. It also uses a shallow neural network as an attention mechanism,[28] which learns to score network edges—in this case, representing atomic interactions—by their importance.

2.1.1 Input Features

Our EGNN takes four inputs: positions, node embeddings, edge indices, and edge embeddings. If there are n atoms in an input structure, the positions tensor is an $n \times 3$ tensor containing the x, y and z coordinates of each atom. The node embeddings are an $n \times 12$ tensor of one-hot encoded OpenBabel atom types, with a bit to distinguish between ligand and receptor atoms. A summary of the five input matrices is shown on the left-hand side of Fig 2.

Edges are generated on-the-fly using a variable distance cutoff. We use a cutoff of 10 Å for ligand-protein edges, and 2 Å for ligand-ligand and protein-protein edges. In this way, intramolecular edges closely mimic the covalent structure of input molecules, with a much more expansive connectivity to describe intermolecular interactions. The edge tensor is an $3 \times m$ matrix of m edges, with one-hot encoding for ligand-ligand, ligand-receptor, and receptor-receptor interactions.

The binding pocket is defined as the collection of protein atoms within 6 Å of any ligand atom; the rest of the protein is ignored.

2.1.2 Training

All models were trained for 10 epochs with a batch size of 32, using the Adam optimiser and cosine warm restarts with a maximum learning rate of 8×10^{-4} and a weight decay of 10^{-4}. For classification models, the selected model is the one with the best Top-1 value on the test set; for regression models, the selected model is the one with the highest Pearson's Correlation Coefficient (PCC) for affinity on the PDBBind Core Set.

For regression models with pretraining, once the classification task is complete, the best model is selected and the final linear layer with sigmoid is replaced by a multi-target regression, where the target is either pK_d, pK_i or pIC_{50}. The labels for the two types of affinity data not present in the training set are ignored for calculating loss, so those weights are unaffected.

2.2 Datasets

Our training dataset for pose classification is Redocked2020[29] (Redocked from hereonin), with the test set generated according to McNutt *et al.*[19] so that classification performance can be directly compared with their work. This test is similar to the *docking power* test from CASF-16,[13] which we also conduct.

For regression on binding affinity values, we train a pose classifier on the Redocked set, finetune on affinity data from the PDBBind General Set, and test on the PDBBind Core Set. This replicates the *scoring power* and *ranking power* tests from CASF-16. As the Core Set is a subset of the General Set, we remove Core Set structures from the training data.

2.2.1 The Redocked Set

Training for pose classification uses the same training data as the Redocked model outlined by McNutt *et al.*[29] In previous work by the same authors,[19] ligands from the Pock-

etome v17.12[30] were redocked using AutoDock Vina into their cognate receptors, with an RMSD calculated between the redocked poses and the crystal pose. Sub-2 Å poses were labelled as active poses, with the rest labelled as inactive. Further negative examples were generated adversarially: a gnina CNN trained on the original redocked dataset was used to optimise docked poses. Optimised poses which were scored highly (> 0.9) by the trained CNN but were more than 2 Å RMSD from the crystal pose were added as inactive poses. In total, there are 52,385 active and 734,417 inactive poses in the version of Redocked2020 used here, which we have shortened to Redocked.

2.2.2 PDBBind Refined: gninaSet$_{Pose}$ Set

The PDBBind refined set v.2019[14] is a carefully selected set of high-quality protein-ligand complexes, complete with binding affinities. In their gnina 1.0 paper,[19] the authors took the 4,852 unique protein-ligand complexes, removing solvents and any other molecules besides the protein and the ligand, as well as removing structures with ligands that do not have a mass between 150 and 1,000 Da. This filtered, preprocessed version of the refined set is hosted by the authors of gnina 1.0[19] at `https://bits.csb.pitt.edu/files/gnina1.0_paper`. Gnina was used with default settings, excepting `--num_modes=50`, `--min_rmsd_filter=0.0`, and the use of the standard Vina scoring function in refinement and ranking rather than a CNN.

Of the 4,260 filtered structures, the 441 which are not used in training the 'redocked' gnina model are selected as the test set for consistency with that work, which we call gninaSet$_{Pose}$. Up to 50 poses are reranked by our GNN (some of which may be very similar), after which the standard 1.0 Å RMSD filter is applied to get a final pose ranking.

2.2.3 PDBBind General and Core Sets

The PDBBind v.2020 General set contains protein-ligand complexes and binding affinities curated from the PDB.[31] The affinities are in the form of pK_d, pK_i or pIC_{50}, and this was the training set for affinity regression. The PDBBind Core set, also known as the CASF-2016 test set for affinity regression, comprises 285 high-quality crystal structures, as well as their binding affinities,[13] and is a subset of the General set. This is the test set for regression (*scoring power* and *ranking power*).

2.2.4 Training dataset filtering

Due to the lack of affinity data, we choose to pretrain on a pose classification task in order to learn some of the physics of binding before finetuning on affinity data. As per Fig 1, filtered subsets of both the Redocked set and the PDBBind v.2020 General Set are generated for both of these stages of training, as well as random subsets of the original training sets of the same size as the filtered sets. The filtered datasets were constructed by removing proteins and ligands if they met either of the following criteria:

1. Tanimoto similarity of the 2048-bit Morgan fingerprint between the ligand and any of the 285 test set ligands is greater than 0.8

2. Sequence identity between the protein and any of the 285 test set proteins is greater than 0.8

These filters were also applied to the Redocked set with respect to the gninaSet$_{Pose}$ test set. All files which could not be parsed by either RDKit[32] or OpenBabel[33] were also discarded.

This process reduces the training set sizes from 780,572 to 633,047 and 629,963 (Redocked\gninaSet$_{Pose80}$ and Redocked\Core$_{80}$) and from 19,157 to 14,555 (General\Core$_{80}$). A full list of datasets is given in Table 1. In order to deconvolute the effects of training set size from the effect of the filters, we also constructed training sets of the same size, randomly sampled from the original training sets. These are called Redocked\gninaSet$_{PoseR}$, Redocked\Core$_R$ and General\Core$_R$. Carrying out filtering in this way should ensure the PDBBind Core set performance is a more accurate reflection of accuracy on unseen targets and ligands.

Dataset	Size	Unique PDB IDs	Task/ Split
Redocked	780,572	19,595	C/Train
Redocked\gninaSet$_{Pose80}$	633,047	17,528	C/Train
Redocked\Core$_{80}$	629,963	16,900	C/Train
General	19,157	19,157	R/Train
General\Core$_{80}$	14,555	14,555	R/Train
gninaSet$_{Pose}$	20,411	411	C/Test
Core	285	285	R/Test

Table 1. Datasets, their sizes and the number of unique PDB structures in their generation. Redocked includes no structures with the same PDB code as any structures in the gninaSet$_{Pose}$ or Core sets, and the General set shares no PDB codes with the Core set. In the Task/Split column, 'C' refers to pose classification and 'R' refers to affinity regression.

2.3 Attribution

It is well documented that the CNNs currently available for virtual screening are prone to distinguishing binders from non-binders based not on protein-ligand interactions, but on ligand features alone.[10–12,34,35] Ensuring that predictive power is diminished in the absence of receptor information in the test set causes at least some receptor information to be used.[36] However, only directly observing which parts of the input space are used in classification can give affirmative proof that machine learning models are learning to identify physical interactions that separate active from inactive poses.

Attribution in machine learning for pose prediction and virtual screening is an ongoing problem; the architecture of most CNNs causes the concept of individual atoms to be lost as information flows deeper into the network, making them fundamentally unsuitable to attribution at the atomic level. By contrast, graph-based architectures such as PointVS maintain distinct nodes (atoms) until the final layers. These, having passed through the entire network, are rich in information and are directly related to the relevant atom in the input. As the node features are directly attributable to their input atom, and the final pose score is a function of the node features, there is a direct relationship between the atoms and the PointVS score, although there is no incentive during training to localise class contributions on particular atoms. The edges between atoms can also be probed for how much importance is ascribed to atomic interactions, as an intuitive way to describe non-covalent bonds. As per Fig 1, we can also use this knowledge of importance assigned by PointVS to bonds to identify important protein atoms for binding.

We use two approaches for attribution: atom masking for gnina, and edge attention for PointVS.

2.3.1 Atom masking with gnina

Masking is a process by which the importance of different atoms can be ascertained. It is carried out by calculating the difference between the score given when an atom i is removed from the set of input atoms, X, and the score when it is present. The importance of atom $i \in X$ is therefore defined as:

$$\text{atom_score}_i = \text{gnina}\,(X) - \text{gnina}\,(X \setminus i)$$

2.3.2 Edge attention attribution with PointVS

Each layer of PointVS has an attention-like mechanism where the edges are given a score between 0 and 1 by a shallow multilayer perceptron (MLP), which takes as input the edge embeddings themselves. The edge message passed to the ith node at each layer $\mathbf{m}_i$ is the sum of connecting edge embeddings $\mathbf{m}_{ij}$ in the neighbourhood of the node $N(i)$, weighted by this attention score e_{ij}, as in Equation 8 in Satorras *et. al*:[27]

$$\mathbf{m}_i = \sum_{j \in N(i)} e_{ij} \mathbf{m}_{ij}$$

The attention weights can be thought of as indicating how much each edge (atom-atom interaction) is weighted by the network.

2.4 Fragment Elaboration

To elaborate a fragment towards more potent, lead-like compounds, information about important areas of the protein pocket being targeted is key. We set up a series of tests to investigate if the attribution scores from PointVS can identify these important sites.

By performing attribution on a crystal structure of a given protein with a small molecule bound, we obtain binding information in the form of an importance score for every protein atom less than 6Å away from any ligand atom. If a fragment screen has been carried out on said target, the attribution process can then be repeated for several crystal structures to obtain an average importance score for each of the protein atoms. We use this list of protein atoms and associated scores as hotspots to perform fragment elaboration. To assess them, we say that the quality of a hotspot— how important the point it is placed on actually is for binding— is proportional to the binding affinity of the molecules generated in the elaboration process, which we assess using a metric derived from docking score, ΔSLE_α.

We compare the ability of PointVS hotspots to highlight important binding regions to traditional, data-based fragment hotspot maps. To obtain these, we use the Hotspots API,[26] which implements the algorithm described in Radoux *et al.*[37] We then process the output of the API as in Hadfield *et al.*[25] A description of this process is given in the SI.

For each target we perform fragment elaboration tests on, we obtain hotspot maps with PointVS using the crystal structures of their fragment screens available on the fragalysis platform.[38] The structures used are listed in SI Table 1. To obtain traditional hotspot maps, we run the Hotspots API on one structure of the target randomly selected from the fragalysis set of bound structures.

We also use the fragalysis set of crystal ligand structures listed in SI Table 1 to obtain fragments to elaborate. To do this, we enumerate all cuts of acyclic single bonds that are not part of functional groups, and add a 'dummy' atom at the site of the cut. This atom is where atoms will be added to the fragment.

To perform fragment elaboration using the two sets of hotspot maps, we use STRIFE, a generative model for fragment elaboration. We follow the method outlined for its use in Hadfield *et al.*[25] We take as input a fragment, a specified exit atom, and information about one hotspot; namely, its coordinates and type. STRIFE then generates molecules matching the pharmacophoric profile specified.

To achieve this, STRIFE has two main stages. The first of these, exploration, aims to generate a set of elaborations which contain an acceptor or donor in close proximity to a hotspot. These elaborations are then docked using GOLD's constrained docking functionality,[3] and those which successfully place a functional group within a certain distance (2Å for the API hotspots, which are in the protein pocket, and 3Å for PointVS hotspots, which are on protein atoms) of the hotspot being targeted are selected as 'quasi-actives'. In the next stage, refinement, these quasi-actives are used to derive a fine-grained pharmacophoric profile. STRIFE then generates elaborations using those pharmacophoric profiles, and docks them. These docked elaborations constitute its final output.

For a given hotspot, we perform elaboration on a set of fragments. The size of this test set depends on the number of bound structures of ligands available for the target in question (see SI Table 1). For some fragment-hotspot pairings, elaborations cannot be generated. This can be due to the hotspot in question being too close or too far from the exit point on the fragment, or at an angle that is unfavourable to elaborate along. In these cases, the generation stage will be unable to produce any quasi-actives; in other words, it will be unable to generate any molecules that, when docked, have a hydrogen bond acceptor or donor within a certain distance from the hotspot. An example of this is shown in Table 5, which shows the number of fragments successfully elaborated in the pocket of Mpro for every hotspot tested. We see that the hotspot ranked ninth by the Hotspots API, for instance, cannot be reached by elaborating on any of the 109 fragments tested, and hence no molecules are output.

The number of final elaborations generated is dependent on the number of quasi-actives that the first stage, exploration, generates. Although STRIFE is asked to generate 250 elaborations per fragment, there are often fragment-hotspot pairings where the number of quasi-actives identified is insufficient for the refinement phase to produce 250 distinct molecules. The mean number of elaborations generated for a given pair is then less than 250, as seen in Table 5. Nevertheless, as each hotspot is tested on a number of fragments occupying various positions in the pocket, we still obtain a large number of generated molecules for a given hotspot.

To assess the generated molecules, we dock them using GOLD,[3] the CCDC's protein-ligand docking software. We use the constrained docking functionality—constraining using the fragment, for which we have a crystal structure—from which each molecule receives a score. We then calculate a ligand efficiency by dividing this score by the number of heavy atoms present in the molecule. This is to compensate for docking algorithms tendencies to favour larger molecules. From the ligand efficiency, we derive a standardised ligand efficiency. This is obtained by standardising the ligand efficiencies of the generated molecules and the ground truth molecule for given fragment-hotspot combination to have zero mean and unit variance (here, ground truth molecule refers to the molecule that was segmented to obtain the test fragment). We then sort the standardised ligand efficiencies of the elaborations from highest to lowest scoring, and take the mean of the top α. In this work, we use α=20. Subtracting the ground truth ligand efficiency value from this value then provides us with ΔSLE_{20} for every fragment-hotspot pair, so for a given hotspot, we take the mean over the ΔSLE_{20}s of all the fragments successfully elaborated towards it. We use this metric as it provides an insight into how the elaboration process when using a particular hotspot has impacted the original molecule's docking score: a positive ΔSLE_{α} means the top elaborations are improvements on the original molecule, and a negative ΔSLE_{α} shows that the elaboration process has decreased the ligand efficiency with respect to the starting molecule.

3. Results

We tested the ability of our MLBSF, PointVS, to perform pose selection and affinity prediction. Through the use of attribution, we also verified not only that PointVS has successfully learnt to recognise binding interactions, but that when given a number of bound structures of a given target, it could be used to extract information about important binding pharmacophores that could then be used in automated fragment elaboration.

3.1 Bias in the CASF-16 Test Set

We implemented a rigorous filtering step to ensure that the training set and test set structures used by PointVS have no overlap (see methods). In order to compare PointVS with other machine learning methods which have not included this filtering step,[19,39,40] we also constructed a smaller test set out of the PDBBind Core set by applying the same filters, but excluding test set structures rather than train set structures. However, we found that such a test set would only contain a single structure: 284 of 285 of the Core set proteins have a counterpart with 90% sequence similarity in the General set. Further, 273 of them (95.7%) have a

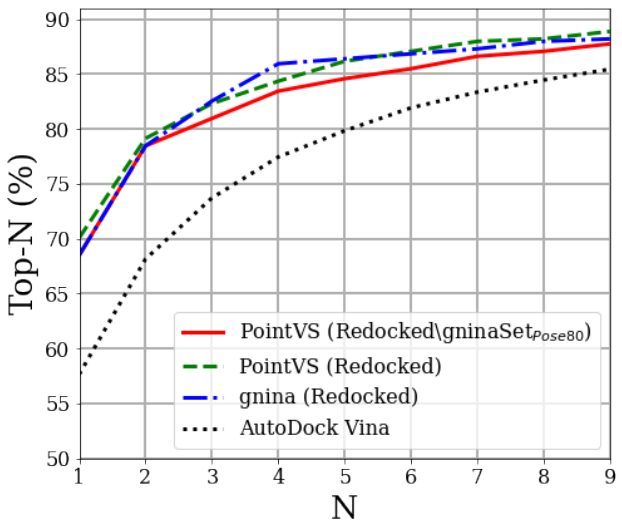

Fig. 3. Top-N vs N pose ranking performance on the gninaSet$_{Pose}$ set for Autodock Vina, PointVS and gnina. Terms in brackets in the legend refer to the training sets; filtering the training set by protein and ligand similarity results in slightly degraded performance. The Top-1 values for PointVS trained on Redocked\gninaSet$_{Pose80}$ and gnina trained on Redocked are the same (68%), with PointVS trained on Redocked achieving 70%.

counterpart with an identical sequence, making any fair and unbiased comparison to these methods impossible.

3.2 Docking Power: Pose Prediction

Docking power refers to a scoring function's ability to identify a ligand's native binding pose among decoys. It is quantified using Top-N, which is the percentage of systems with a "good" pose ranked in the top N. A pose is considered good if the RMSD to the crystal pose is less than 2Å .

Top-N pose ranking performance on the gninaSet$_{Pose}$ set is shown in Fig 3. When the training sets are the same, PointVS ranks a good pose at the top in 70% of cases, as opposed to 68% with gnina. When PointVS is trained on the smaller Redocked\gninaSet$_{Pose80}$ set, such that no similar proteins or ligands as the test set are seen during training, this drops to 68%. This suggests that for pose prediction, filtering the dataset to remove overlap between train and test structures only causes a minor decrease in docking power.

The Top-1 pose ranking results for the Core set (the CASF-16 docking power set) are shown in Table 2, for both the case where the crystal pose is included amongst the poses to be ranked, and the case where it is not.

The difference in performance between all of the methods

	Top-1	
Model	Crystal pose included	Crystal pose not included
PointVS (Redocked\Core$_R$)	90.5	84.9
PointVS (Redocked\Core$_{80}$)	91.2	84.2
PointVS (Redocked)	**91.3**	**85.3**
gnina (Redocked)	91.2	83.2
Autodock Vina	90.2	84.6

Table 2. Top-1 pose ranking performance for different models and training sets (in brackets) on the PDBBind Core set (the CASF-16 docking power test set). The non-machine learning scoring function is shown in italic. The performance is shown for both the case where the crystal structure of the ligand is included in the set of poses being ranked, and the case where it is not included, in which case the native pose is defined as any pose less than 2Å RMSD away from the crystal pose. The highest Top-1 for each case is shown in bold.

is minimal, and is not affected significantly by whether or not the training data has been filtered for structural similarity (the without-ligand test set scores are 85.3%, 84.9% and 84.2% for PointVS trained on Redocked, Redocked\Core$_R$ and Redocked\Core$_{80}$, respectively). This lack of dependence on debiasing is in agreement with the docking power results shown in Fig 3, although the performance of Autodock Vina is comparable with the machine learning methods in this test.

3.3 Scoring Power: Affinity Prediction

The scoring power is defined by Su *et al.* as "the ability of a scoring function to produce binding scores in a linear correlation with experimental binding data".[13] This is best measured using the Pearson correlation coefficient (PCC) between the score given by the scoring function and the measured binding affinity data. For training our networks, we once again used both filtered and unfiltered versions of the PDBBind General dataset to to test the influence of dataset bias.

We trained PointVS to classify on Redocked\Core$_{80}$, and then switched out the final layer for multi-target regression trained on General\Core$_{80}$. We also used the gnina model trained on the PDBBind General set supplied as part of work by McNutt *et al.*[19] to find the PCC on the Core set, but again emphasise that the training data for this model includes many proteins and ligands which are similar or identical to those in the Core set. This model

	Scoring Function	PCC
Biased	gnina (Redocked)	0.753 ± 0.008
	gnina (General)	$\mathbf{0.816 \pm 0.008}$
	PointVS (General)	0.805 ± 0.010
	PointVS (General\Core$_R$)	0.803 ± 0.012
	ΔVinaXGB	0.796
	ΔVinaRF	0.732
Debiased	PointVS (General\Core$_{80}$)	$\mathbf{0.754 \pm 0.015}$
	X-Score	0.631
	Autodock Vina	0.601

Table 3. Pearson correlation coefficients between measured and predicted affinity for different scoring functions on the PDBBind Core set. Scoring functions are split into biased and debiased methods according to the overlap between their training sets, which are shown in brackets where applicable, and the Core set. Non-machine learning scoring functions are shown in italic. The highest PCCs obtained with both biased and debiased methods are shown in bold.

achieves a PCC of 0.816. The results from other methods can be seen in Table 3. The three best methods without dataset filtering (gnina, PointVS and ΔVinaXGB) achieve very similar performance, and PointVS outperforms the best non-machine-learning methods from the original CASF-16 work,[13] Autodock Vina, significantly (0.805 vs 0.601). However, the performance of PointVS when trained on the filtered dataset General\Core$_{80}$ is a better indicator of its true performance on unseen protein-ligand combinations with no analogues in the training data.

The three machine learning methods which use three distinct featurisation methods and three separate architectures (PointVS, gnina and ΔVinaXGB) obtain similar PCCs when trained on the unfiltered General set. This suggests that the limiting factor in predictive performance is what information the training data holds about the test set data, rather than the architecture or featurisation.

To test whether the drop in the performance of PointVS when similar structures are removed from the training set is related to bias or change in training data size, we trained PointVS on General\Core$_R$. This has the same training set size as General\Core$_{80}$, but can still contain similar structures to those in the test set. PointVS trained on the General\Core$_R$ achieves a PCC of 0.803 on the CASF-16 set. This is almost identical to the PCC of PointVS trained on the entire General set (PCC of 0.805), and significantly higher than PointVS trained on the General\Core$_{80}$ set (PCC of 0.754). This once again points to the performance of these methods when trained and tested using biased datasets being boosted. This contrasts with our findings in pose prediction performance, in which we saw very minimal change when filtering was performed.

As PointVS trained and tested in a debiased way still appears to be predictive of binding affinity, we next explored whether it had learnt to identify important interactions in the binding site.

3.4 Attribution: Identifying Important Sites

PointVS appears to offer a substantial improvement in predictive performance of binding affinity over non-machine-learning methods. However, MLBSFs are notoriously difficult to interpret. Good performance when trained on debiased training data is circumstantial evidence that the interatomic interactions involved in binding are being learned, but demonstrating that the attribution scores of PointVS relate to important binding interactions would be more concrete. GNNs are well-suited to this kind of analysis, and we next present several results demonstrating that important interatomic interactions have been learnt by PointVS.

3.4.1 Human Tankyrase-2 Inhibitors

The Protein-Ligand Interaction Profiler (PLIP)[41] uses simple geometric rules to predict interactions at the interface between a protein and a ligand. We used PLIP to identify the "most important" bonds for three human Tankyrase-2 inhibitors, and examined whether the atoms forming these bonds were highlighted when attribution was carried out on gnina[19] and PointVS.

In their paper on attribution with gnina,[24] the authors described various methods to overcome the difficulties associated with performing attribution on a CNN. However, the code implementing these methods, gninavis, is currently unavailable, so we instead implemented a standard atomic masking procedure (see methods).

The structures of three tankyrase inhibitors are shown in Fig 4. The leftmost column (structures a, d and g) shows the PLIP analysis of each structure. The structures in the other two columns show the results of attribution with gnina (centre, structures b, e and h) and PointVS (right, structures c, f and i). The structures in the central column are thus coloured by the attribution scores obtained from masking with gnina, with atoms contributing negatively to binding being shown in red (negative score), neutral atoms in white, and positively-contributing atoms in green (positive score). Attribution with PointVS was carried out using edge attention, and thus the attribution scores produced correspond to interactions between pairs of atoms rather than individual atoms. The five highest-scoring edges are shown in

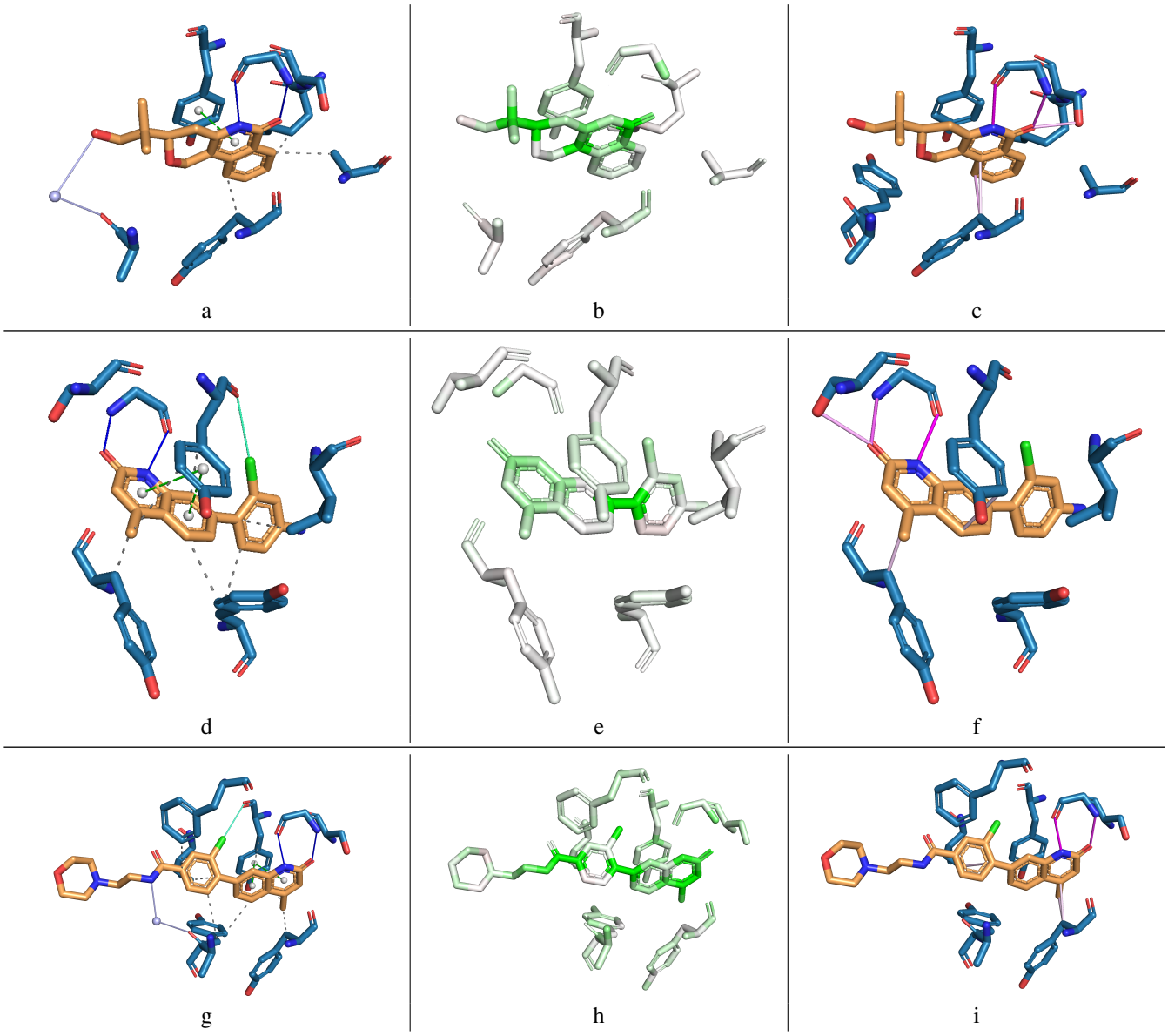

Fig. 4. Three Tankyrase-2 inhibitors: 5C5P (a, b, c), 4J21 (d, e, f), and 4J22 (g, h, i). The leftmost column shows the Protein-Ligand Interaction Profiler (PLIP) analysis of each structure, where dark blue lines are hydrogen bonds, dotted grey are hydrophobic interactions, dotted green are π-π interactions, solid green are halogen bonds, and lilac are water bridges. The central column shows the results of performing masking with gnina, with green representing a positive attribution score (identified as making a positive contribution to binding) and red a negative score (making a negative contribution). The rightmost column shows the results of edge-attention attribution performed with PointVS, with the lines between atoms showing the top five highest-scoring edges for each structure, with darker pink representing higher scores.

structures c, f and i, with dark pink lines representing high scores, and lighter pink representing lower scores.

Considering the first row, the two ligand atoms that form hydrogen bonds with the protein as calculated by PLIP (Fig 4a) are scored by gnina as the 6th and 8th most important of 20 (Fig 4b). Of the two hydrogen bonding protein atoms, gnina recognises one of them as being extremely important (the highest scoring protein atom), and the other as neutral. For the second structure, Fig 4e shows a similar story, with the three important ligand atoms as given by PLIP (Fig 4d) scoring 4th, 7th and 8th out of 20, but the protein atoms they respectively bind to scoring negatively, neutrally and very slightly positively. In the third structure, the three bound ligand atoms as identified by PLIP (Fig 4g) are scored 11th, 13th and 14th of 30 ligand atoms, with the corresponding protein atoms scoring negatively, weakly positively and moderately positively (Fig 4h). Interestingly, the last two structures both contain halogen bonds, and in both cases gnina ranks the ligand atom as important, and the protein atom as a negative contribution. Overall, gnina struggles to identify important individual atoms (both in the ligand and protein) for binding. The atoms being scored individually rather than by pairs as with edge attention makes it more difficult to identify the bonds that are being formed: of the bonds identified by PLIP, only in the first structure was there an example where both the protein and ligand atoms were given a high score by gnina, making it the only case where an important bond was identified.

When we performed atom masking on PointVS, we found that the results were similar to those from gnina, in that the atoms contributing to bonds were scored highly but not necessarily enough to recognise their true importance. However, we found that edge attention analysis provided a clearer insight into important interactions.

Considering the first example in Fig 4, we see that the bonds ranked first and second most important by PointVS (Fig 4c) correspond to the hydrogen bonds identified by PLIP (Fig 4a). Edges between the two aromatic rings involved in π-stacking are also given high importance scores, being ranked fourth and fifth most important. We see a similar pattern for the second structure, where the atoms involved in hydrogen bonds as defined by PLIP (Fig 4d) are connected by edges assigned high importance by PointVS (ranked first and second most important, Fig 4f). We also again see high scores assigned to the edges connecting the rings involved in π-stacking. PointVS does, however, fail to recognise the edge joining the atoms involved in the halogen bond shown in green in Fig 4d. In the third example structure, PointVS also identifies the hydrogen bonds identified by PLIP (Fig 4g) as being important, again ranking them as the most and second most important edges (Fig 4i). The other edges assigned high importance correspond to hydrophobic interactions. These results suggest that the edge attribution scores from PointVS are able to identify important binding interactions.

	PointVS		gnina	
	PCC	ρ	PCC	ρ
Top 5	-0.710	0.640	-0.233	0.234
Top 10	-0.853	0.788	0.094	0.093

Table 4. Mean PCCs calculated between the scores of the top five and top ten ranked protein atoms by PointVS, and the distance between them and the nearest ligand atom. Also shown is the mean rank correlation calculated between these values, ρ. The means were calculated over a subset of 20 randomly selected bound structures from the PDBBind Core set (see SI for PDB IDs).

3.4.2 Large Scale Attribution Tests

To further verify that performing attribution with PointVS results in similar bonds being highlighted to those specified by PLIP, we performed attribution on the PDBBind Core set (the CASF-16 test set). We calculated the PCC between the scores assigned to the top five and top ten scoring protein atoms, and the distance between the protein atom and the corresponding ligand atom. This results in a PCC of -0.766 for the top five protein atoms, and -0.844 for the top ten protein atoms. This negative correlation implies that protein-ligand atom pairs that are close together (which in turn PLIP will consider more likely to be forming a bond) are commonly identified by PointVS. We also calculated the correlation coefficient between the ranks of the top five and ten protein atoms and their distance-based rank (this corresponds to the protein atoms ranked by distance to the nearest ligand atom), and obtain 0.719 and 0.788, respectively.

We carried out this process for gnina, but as masking is a significantly more computationally challenging process than edge attention analysis, we used only 20 randomly selected structures from the Core set (see SI for list of PDB IDs). We also performed attribution with PointVS on this subset for comparison. The results of calculating both the PCC and the rank correlation, ρ, are shown in Table 4.

On this smaller set we again see a negative correlation between the score assigned by PointVS and the distance between the atoms, and a positive correlation between their rankings by distance and PointVS. When using gnina, by contrast, we see a much weaker correlation for both of these tests.

These results once again suggest that PointVS is capable

of identifying bonds that at minimum make sense geometrically, providing further evidence that the edge attribution scores from PointVS are identifying important binding interactions.

3.5 Hotspot Identification using PointVS

Having shown that PointVS is potentially capable of identifying important binding interactions, we next assessed whether it can be used as a method for extracting structural information from a number of bound structures, and hence used to guide molecule design. To do this, we extracted hotspot maps from PointVS by performing edge attention attribution on fragment screen data, and compared the resulting hotspots to those found using a data-driven approach, the Hotspots API.[26]

Our first test used the bound structures available for the SARS-CoV-2 main protease (Mpro). The dataset available for this target is far more extensive than most targets will benefit from, as it is comprised of not only fragment-like molecules, but also follow-up compounds. These follow-up compounds, which have been curated with the specific intention of targetting important protein atoms, consist of closely related compounds with the same basic scaffold. Intuitively, the presence of high-quality compounds should result in PointVS being able to extract higher-quality hotspots, as the bound ligands were designed to interact with protein atoms that have been experimentally validated to be important. We used this dataset as a starting point to verify that, given a selection of bound structures, PointVS can be used to identify these important protein atoms in a way that is useful for fragment elaboration.

The data was extracted from the fragalysis platform.[42] A full list detailing the structures used is given in SI Table 1. The hotspots identified by the Hotspots API and attribution with PointVS are shown in Fig 5a and b. The hotspots of the two methods will not fall on exactly the same points, as the PointVS hotspots correspond to protein atoms, and the API hotspots to points in the binding pocket. Still, the two methods clearly highlight very separate regions of the binding pocket as important.

3.5.1 Impact of Fragment Screen Similarity

As mentioned previously, the Mpro dataset contains a significant number of closely-related follow-up compounds with the same basic scaffold. To ensure that PointVS is providing a novel insight into important binding regions in the pocket of Mpro and not highlighting important protein atoms by simply counting the number of times they are within close proximity of a ligand donor or acceptor atom, we used PLIP—which does use simple geometric rules to predict interactions—to extract the protein atoms that could be forming hydrogen bonds with ligand atoms for every bound structure. We then defined any protein atom that was highlighted more than five times across the 152 bound structures as a PLIP hotspot. This cutoff of five interactions resulted in only four hotspots being extracted. These top four are shown in Fig 5c, and correspond to protein atoms that were highlighted by PLIP 146, 40, 9 and 5 times out of the possible 152.

All but one of the PLIP hotspots are within 2Å of one of the top five PointVS hotspots. However, the top-ranking PLIP hotspot (which corresponds to a protein atom that forms a hydrogen bond in 146 of the 152 bound structures) is ranked second by PointVS, and the second PLIP hotspot (which PLIP identifies as interacting with ligand atoms in 40 structures) is ranked top by PointVS. As the first PLIP hotspot is at most the length of one hydrogen bond away from a ligand acceptor in almost every structure, we would expect a geometry-based method to clearly identify it as the top hotspot, as PLIP does. This is some evidence that PointVS is identifying important protein atoms with a more nuanced approach than simply counting interactions identified with geometric rules. These results do not mean the PointVS hotspot extraction method is immune to being biased when supplied with fragment screens containing clusters of ligand donor and acceptor atoms—however, it is a promising sign that it is not entirely biased by such clusters, and that PointVS is still able to see past them and identify other areas in the pocket as important. This is a particularly useful finding given that recent research into fragment screen libraries has highlighted that even screens designed to be diverse structurally offer a limited exploration of protein pockets.[43]

3.5.2 Dependency on Fragment Screen Size

Given that PointVS identifies sites that are different from a traditional hotspot method and a geometry-based method, we next tested whether the high-scoring sites identified by PointVS are dependent on the size of the input fragment set.

To do this, we performed the same hotspot extraction process as before, but instead of using all the fragment screen data (SI Table 1) at once, we randomly sampled smaller sets from it. We varied the size of the set sampled between 10 and 80. We then took the top five highest-scoring hotspots generated using PointVS with each randomly sampled set of fragment hits. The results of this are shown in Fig 6, where we took samples of size 10, 30 and 80 from the available bound structures (further images using other dataset sizes are given in SI Fig 2). This random sampling process was carried out 40 times. We see that when the hotspot maps are extracted from a smaller number of bound structures, a

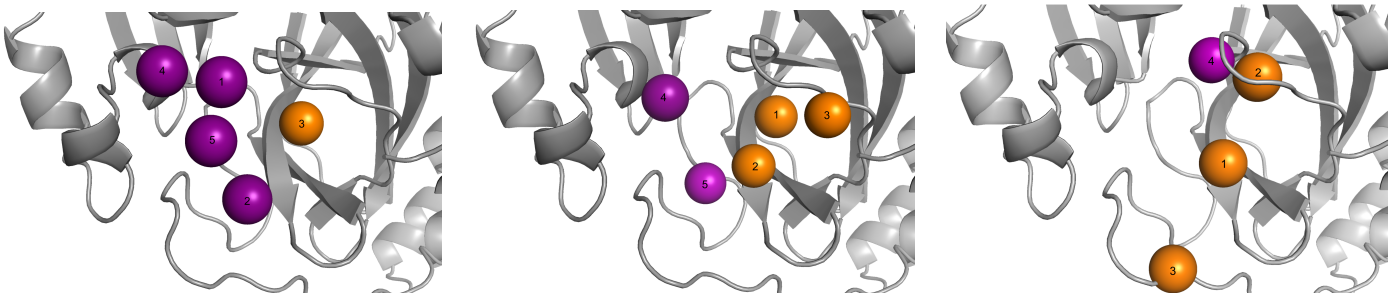

Fig. 5. Donor and acceptor hotspot maps in the binding pocket of Mpro, coloured purple and orange respectively, and numbered according to their rank. The hotspots on the left (a) were obtained with the Hotspots API, the hotspots in the centre (b) were obtained with PointVS by performing attribution on 152 structures of bound fragments, and the hotspots on the right (c) were obtained by extracting the most common protein atoms identified by PLIP as involved in hydrogen bonds with ligand atoms across the 152 bound structures (in this case identified over five times).

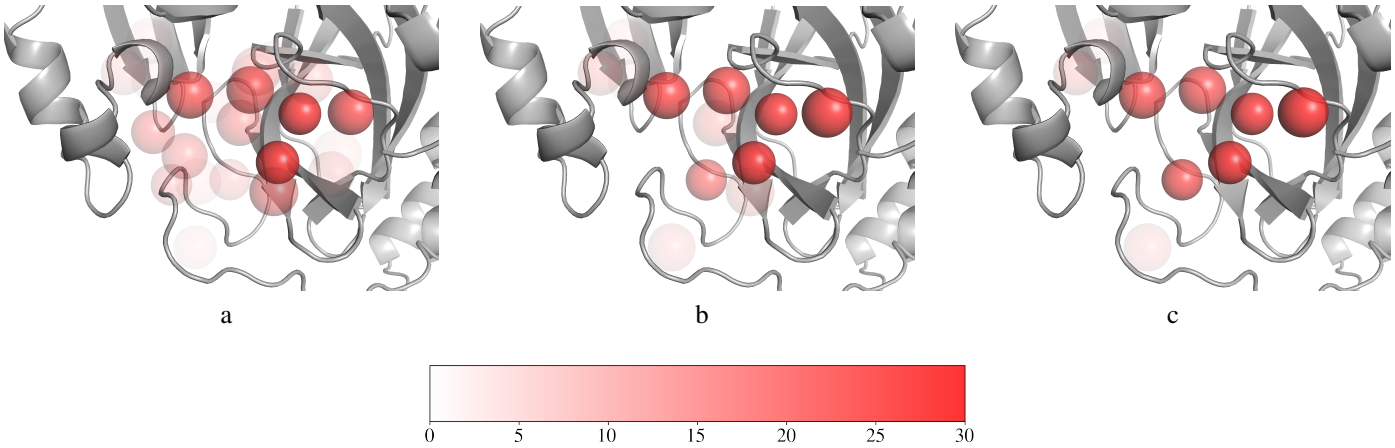

Fig. 6. Top five scoring hotspot maps in the binding pocket of Mpro found by performing attribution on 40 sets of randomly sampled sets of 10 (a), 30 (b) and 80 (c) bound structures. Both donor and acceptor hotspots are shown in red. The spheres representing the hotspots are transparent and overlaid, so the more opaque a hotspot appears, the more times it was ranked in the top five.

wider range of protein atoms are identified as being important; PointVS is less able to consistently pick out the same five protein atoms every time, and increasing the number of bound structures given to PointVS results in more consistent hotspot maps being generated. Nevertheless, we note that even when using the smallest datasets containing only 10 bound structures, the five hotspots that are identified when using the full fragment screen are the most commonly included, hence their darker colour in Fig 6. This is a promising sign that attribution with PointVS could also be a useful tool for less well-studied targets.

3.6 Fragment Elaboration

Having demonstrated that the PointVS hotspots are consistent amongst themselves, and that they highlight different areas in the Mpro binding site to the API hotspots, we assessed whether they correctly highlight important areas by performing fragment elaboration. If PointVS is successfully identifying important interactions, molecules generated to satisfy the pharmacophoric constraints imposed by PointVS hotspots should be as good, if not better, than the molecules using the API hotspots.

We performed attribution on the full set of Mpro bound crystal structures (SI Table 1) to obtain PointVS hotspot maps, and used the Hotspots API to obtain a second set of hotspot maps. We used each of the top ten ranked hotspots from each set of maps to elaborate on 109 fragments. The number of fragments that were successfully elaborated—referring to cases where STRIFE was successfully able to grow towards the hotspot, and the donor or acceptor atom placed remained near to the hotspot after docking—using each hotspot is shown in Table 5, alongside the mean number of elaborations made per fragment.

To assess the binding affinity of the generated elaborations, we docked them, as well as the fragment they were grown from, and used both docking scores to calculate a standardised ligand efficiency score, ΔSLE. This is the difference in ligand efficiency between the starting fragment and the elaborated compound (see methods). We then ranked the elaborations by these scores, and took the average of the top 20 scores to obtain ΔSLE_{20}. To see the performance of a hotspot over all fragments successfully elaborated with it, we took the mean of the ΔSLE_{20}s obtained.

The highest scoring elaborations by our ΔSLE_{20} metric were generated using the top five PointVS hotspots (Table 6). Elaborations made using the hotspots ranked 6-10 by PointVS have worse ΔSLE_{20}s. By contrast, the Hotspots API successfully identified ten high-scoring hotspots (indeed, on average, these top ten hotspots produced elaborations with higher standardised ligand efficiencies than the PointVS hotspots), but was unable to successfully rank them amongst themselves. The accurate ranking of hotspots is important, as in real-world fragment-to-lead campaigns, only a small number of them can easily be targeted.

To test whether PointVS hotspots are also reliable for other proteins, we repeated the above process for two other targets: SARS-CoV-2 non-structural protein 3 (Mac1),[44] and SARS-CoV-2 non-structural protein 14 (NSP14).[45] These both have fragment screen datasets available on fragalysis[46,47] (see SI Table 1). In both cases, these are considerably smaller than the Mpro dataset, and do not contain follow-up compounds.

Each of the top ten hotspots produced by PointVS and the API were tested, the results of which are shown in Table 7. Both sets of hotspots for Mac1 and NSP14 were tested on 35 and 30 fragments, respectively. The number of successfully elaborated fragments and mean number of elaborations generated per fragment for these targets are provided in SI Table 2.

On average, the standardised ligand efficiency of molecules generated with PointVS hotspot maps is greater than those generated with the API hotspots. Within the PointVS scores, we see that the Mpro hotspots are lower scoring than those for the other two targets. This can be attributed to the 109 starting fragments for Mpro being of higher quality, having been extracted from curated follow-up compounds rather than fragments. The improvement that is made on them by elaborating is thus less significant. We also see that, unlike with the Hotspots API, the hotspots ranked 1-5 by PointVS consistently outperform those ranked 6-10, suggesting that the attribution method is good not only at picking out important atoms, but also ranking them amongst themselves.

4. Conclusion

In this paper we described the development of PointVS, a state of the art EGNN based method for affinity prediction, and the first ML-based method for extracting important binding information from a target for molecule design.

During the development of PointVS we also identified that a commonly used benchmark for MLBSFs, CASF-16, overestimates their accuracy when trained using the most commonly used training dataset. In light of this, PointVS was trained and tested on a rigorously filtered dataset, and hence encouraged to learn the rules governing intermolecular binding rather than memorise training data. We showed that when trained on this filtered dataset, PointVS achieves comparable results to other leading scoring functions, providing some evidence that it is successfully identifying im-

	PointVS		Hotspots API	
Rank	Fragments successfully elaborated	Elaborations per fragment	Fragments successfully elaborated	Elaborations per fragment
1	57	215	26	189
2	82	182	57	183
3	51	202	59	207
4	14	199	9	158
5	21	223	28	179
6	60	183	23	162
7	46	228	3	220
8	78	216	54	197
9	24	215	0	0
10	47	218	28	179

Table 5. The number of fragments that were successfully elaborated on using PointVS and API hotspots for Mpro, and the mean number of elaborations that were generated for each fragment. STRIFE was provided with 109 fragments to elaborate on for each hotspot, and asked to generate 250 elaborations for each one.

Method	PointVS	API
Hotspots 1-5: ΔSLE_{20}	**0.304**	0.213
Hotspots 6-10: ΔSLE_{20}	0.146	**0.269**

Table 6. The mean standardised ligand efficiency of the top 20 highest-scoring molecules (ΔSLE_{20}) generated using hotspots ranked 1-5 and 6-10 by PointVS and the Hotspots API for Mpro. The highest ΔSLE_{20} for both ranges of hotspots is shown in bold.

portant binding interactions. We provided further proof of this by performing attribution, and showed that PointVS is able to identify important interactions in line with those found by PLIP, a distance-based tool for profiling protein-ligand interactions.

Finally, we investigated how knowledge of important binding regions could be leveraged in other stages of the drug development pipeline; namely fragment elaboration. We showed that when provided with a set of bound structures, performing attribution on such structures yielded hotspot maps describing important protein atoms. Using these in unison with a fragment elaboration tool, STRIFE, resulted in improved docking scores for the elaborated molecules compared to when hotspots were obtained with a data-based method. This is further evidence that PointVS is not learning to memorise ligand information but to recognise important interactions, and additionally constitutes the first ML-based method of extracting structural information from a protein target in a way that is useful for fragment elaboration. More broadly, our work demonstrates that attribution techniques, when applied to debiased models, can be useful for extracting structural information in a way that can be useful in molecule generation.

5. Acknowledgements

This research was funded by the British Biological Sciences Research Council, the Engineering and Physical Sciences Research Council, BenevolentAI, and IBM Research. It was additionally supported by the Rosetrees Trust (Ref M940).

BIBLIOGRAPHY

[1] O. J. Wouters, M. McKee, and J. Luyten, "Estimated Research and Development Investment Needed to Bring a New Medicine to Market, 2009-2018," *JAMA*, vol. 323, pp. 844–853, 03 2020.

[2] G. M. Morris, R. Huey, W. Lindstrom, M. F. Sanner, R. K. Belew, D. S. Goodsell, and A. J. Olson, "Autodock4 and autodocktools4: Automated docking with selective receptor flexibility," *Journal of Computational Chemistry*, vol. 30, no. 16, pp. 2785–2791, 2009.

[3] M. L. Verdonk, J. C. Cole, M. J. Hartshorn, C. W. Murray, and R. D. Taylor, "Improved protein–ligand docking using gold," *Proteins: Structure, Function, and Bioinformatics*, vol. 52, no. 4, pp. 609–623, 2003.

[4] C. Shen, J. Ding, Z. Wang, D. Cao, X. Ding, and T. Hou, "From machine learning to deep learning: Advances in scoring functions for protein–ligand docking," *WIREs Computational Molecular Science*, vol. 10, no. 1, p. e1429, 2020.

[5] D. Jones, H. Kim, X. Zhang, A. Zemla, G. Stevenson, W. F. D. Bennett, D. Kirshner, S. E. Wong, F. C. Light-

	Mpro: 152		Mac1: 58		NSP14: 19	
ΔSLE_{20}	PointVS	API	PointVS	API	PointVS	API
Hotspots 1-5	**0.341**	0.213	**1.749**	1.581	**1.708**	1.240
Hotspots 6-10	0.189	**0.269**	1.727	**1.748**	**1.143**	1.193

Table 7. Mean standardised ligand efficiency of the top 20 elaborations (ΔSLE_{20}) made using PointVS hotspots and API hotspots on three different targets: Mpro, Mac1, and NSP14. The numbers after the target names refer to the number of bound fragment structures available for each target. The list of fragalysis codes corresponding to the structures used is given in SI Table 1. The highest ΔSLE_{20} for both ranges of hotspots is shown in bold.

stone, and J. E. Allen, "Improved protein–ligand binding affinity prediction with structure-based deep fusion inference," *Journal of Chemical Information and Modeling*, vol. 61, no. 4, pp. 1583–1592, 2021. PMID: 33754707.

[6] K. Hornik, M. Stinchcombe, and H. White, "Multilayer feedforward networks are universal approximators," *Neural Networks*, vol. 2, no. 5, pp. 359–366, 1989.

[7] V. Chenthamarakshan, P. Das, S. Hoffman, H. Strobelt, I. Padhi, K. W. Lim, B. Hoover, M. Manica, J. Born, T. Laino, and A. Mojsilovic, "Cogmol: Target-specific and selective drug design for covid-19 using deep generative models," in *Advances in Neural Information Processing Systems* (H. Larochelle, M. Ranzato, R. Hadsell, M. Balcan, and H. Lin, eds.), vol. 33, pp. 4320–4332, Curran Associates, Inc., 2020.

[8] S. C. Hoffman, V. Chenthamarakshan, K. Wadhawan, P.-Y. Chen, and P. Das, "Optimizing molecules using efficient queries from property evaluations," *Nature Machine Intelligence*, vol. 4, no. 1, 2021.

[9] F. Boyles, C. M. Deane, and G. M. Morris, "Learning from docked ligands: Ligand-based features rescue structure-based scoring functions when trained on docked poses," *Journal of Chemical Information and Modeling*, vol. 0, no. 0, p. null, 0. PMID: 34469150.

[10] J. Sieg, F. Flachsenberg, and M. Rarey, "In need of bias control: Evaluating chemical data for machine learning in structure-based virtual screening," *Journal of Chemical Information and Modeling*, vol. 59, no. 3, pp. 947–961, 2019.

[11] L. Chen, A. Cruz, S. Ramsey, C. J. Dickson, J. S. Duca, V. Hornak, D. R. Koes, and T. Kurtzman, "Hidden bias in the dud-e dataset leads to misleading performance of deep learning in structure-based virtual screening," *PLOS ONE*, vol. 14, no. 8, p. e0220113, 2019.

[12] I. Wallach and A. Heifets, "Most ligand-based classification benchmarks reward memorization rather than generalization," *Journal of Chemical Information and Modeling*, vol. 58, no. 5, pp. 916–932, 2018. PMID: 29698607.

[13] M. Su, Q. Yang, Y. Du, G. Feng, Z. Liu, Y. Li, and R. Wang, "Comparative assessment of scoring functions: The casf-2016 update," *Journal of Chemical Information and Modeling*, vol. 59, no. 2, pp. 895–913, 2019.

[14] Z. Liu, M. Su, L. Han, J. Liu, Q. Yang, Y. Li, and R. Wang, "Forging the basis for developing protein–ligand interaction scoring functions," *Accounts of Chemical Research*, vol. 50, no. 2, pp. 302–309, 2017. PMID: 28182403.

[15] J. Yosinski, J. Clune, A. Nguyen, T. Fuchs, and H. Lipson, "Understanding neural networks through deep visualization," *arXiv preprint arXiv:1506.06579*, 2015.

[16] W. Samek, A. Binder, G. Montavon, S. Lapuschkin, and K.-R. Müller, "Evaluating the visualization of what a deep neural network has learned," *IEEE transactions on neural networks and learning systems*, vol. 28, no. 11, pp. 2660–2673, 2016.

[17] C. Poelking, G. Chessari, C. W. Murray, R. J. Hall, L. Colwell, and M. Verdonk, "Meaningful machine learning models and machine-learned pharmacophores from fragment screening campaigns," 2022.

[18] B. Sharma, V. Chenthamarakshan, A. Dhurandhar, S. Pereira, J. A. Hendler, J. S. Dordick, and P. Das, "Accurate clinical toxicity prediction using multi-task deep neural nets and contrastive molecular explanations," 2022.

[19] A. T. McNutt, P. Francoeur, R. Aggarwal, T. Masuda, R. Meli, M. Ragoza, J. Sunseri, and D. R. Koes, "Gnina 1.0: molecular docking with deep learning," *Journal of Cheminformatics*, vol. 13, no. 1, 2021.

[20] L. Zheng, J. Fan, and Y. Mu, "Onionnet: a multiple-layer intermolecular-contact-based convolutional neural network for protein–ligand binding affinity prediction," *ACS Omega*, vol. 4, no. 14, pp. 15956–15965, 2019. PMID: 31592466.

[21] Y. Li, M. A. Rezaei, C. Li, and X. Li, "Deepatom: A framework for protein-ligand binding affinity prediction," in *2019 IEEE International Conference on Bioinformatics and Biomedicine (BIBM)*, pp. 303–310, 2019.

[22] E. N. Feinberg, D. Sur, Z. Wu, B. E. Husic, H. Mai, Y. Li, S. Sun, J. Yang, B. Ramsundar, and V. S. Pande, "Potentialnet for molecular property prediction," *ACS central science*, vol. 4, no. 11, pp. 1520–1530, 2018.

[23] J. A. Morrone, J. K. Weber, T. Huynh, H. Luo, and W. D. Cornell, "Combining docking pose rank and structure with deep learning improves protein–ligand binding mode prediction over a baseline docking approach," *Journal of Chemical Information and Modeling*, vol. 60, no. 9, pp. 4170–4179, 2020. PMID: 32077698.

[24] J. Hochuli, A. Helbling, T. Skaist, M. Ragoza, and D. R. Koes, "Visualizing convolutional neural network protein-ligand scoring," *Journal of Molecular Graphics and Modelling*, vol. 84, pp. 96–108, 2018.

[25] T. E. Hadfield, F. Imrie, A. Merritt, K. Birchall, and C. M. Deane, "Incorporating target-specific pharmacophoric information into deep generative models for fragment elaboration," *Journal of Chemical Information and Modeling*, vol. 62, no. 10, pp. 2280–2292, 2022. PMID: 35499971.

[26] P. R. Curran, C. J. Radoux, M. D. Smilova, R. A. Sykes, A. P. Higueruelo, A. R. Bradley, B. D. Marsden, D. R. Spring, T. L. Blundell, A. R. Leach, W. R. Pitt, and J. C. Cole, "Hotspots api: A python package for the detection of small molecule binding hotspots and application to structure-based drug design," *Journal of Chemical Information and Modeling*, vol. 60, no. 4, pp. 1911–1916, 2020. PMID: 32207937.

[27] V. G. Satorras, E. Hoogeboom, and M. Welling, "E(n) equivariant graph neural networks," 2021.

[28] A. Vaswani, N. Shazeer, N. Parmar, J. Uszkoreit, L. Jones, A. N. Gomez, L. u. Kaiser, and I. Polosukhin, "Attention is all you need," in *Advances in Neural Information Processing Systems* (I. Guyon, U. V. Luxburg, S. Bengio, H. Wallach, R. Fergus, S. Vishwanathan, and R. Garnett, eds.), vol. 30, Curran Associates, Inc., 2017.

[29] P. G. Francoeur, T. Masuda, J. Sunseri, A. Jia, R. B. Iovanisci, I. Snyder, and D. R. Koes, "Three-dimensional convolutional neural networks and a cross-docked data set for structure-based drug design," *Journal of Chemical Information and Modeling*, vol. 60, no. 9, pp. 4200–4215, 2020. PMID: 32865404.

[30] I. Kufareva, A. V. Ilatovskiy, and R. Abagyan, "Pocketome: an encyclopedia of small-molecule binding sites in 4d," *Nucleic Acids Research*, vol. 40, no. D1, pp. D535–D540, 2011.

[31] S. K. Burley, C. Bhikadiya, C. Bi, S. Bittrich, L. Chen, G. V. Crichlow, C. H. Christie, K. Dalenberg, L. Di Costanzo, J. M. Duarte, S. Dutta, Z. Feng, S. Ganesan, D. S. Goodsell, S. Ghosh, R. K. Green, V. Guranović, D. Guzenko, B. P. Hudson, C. L. Lawson, Y. Liang, R. Lowe, H. Namkoong, E. Peisach, I. Persikova, C. Randle, A. Rose, Y. Rose, A. Sali, J. Segura, M. Sekharan, C. Shao, Y.-P. Tao, M. Voigt, J. D. Westbrook, J. Y. Young, C. Zardecki, and M. Zhuravleva, "RCSB Protein Data Bank: powerful new tools for exploring 3D structures of biological macromolecules for basic and applied research and education in fundamental biology, biomedicine, biotechnology, bioengineering and energy sciences," *Nucleic Acids Research*, vol. 49, pp. D437–D451, 11 2020.

[32] G. Landrum, P. Tosco, B. Kelley, Ric, sriniker, gedeck, R. Vianello, NadineSchneider, E. Kawashima, A. Dalke, D. N, B. Cole, D. Cosgrove, M. Swain, S. Turk, AlexanderSavelyev, G. Jones, A. Vaucher, M. Wójcikowski, D. Probst, V. F. Scalfani, guillaume godin, A. Pahl, F. Berenger, JLVarjo, K. Ujihara, strets123, JP, DoliathGavid, and G. Sforna, "rdkit/rdkit: 2021_09_4 (q3 2021) release," Jan. 2022.

[33] G. Hutchison, baoilleach, T. Vandermeersch, chrismorl, R. Danne, M. Banck, M. D. Hanwell, D. Lonie, D. Fomichev, M. Swain, jbrefort, K. Tokarev, D. Koes, P. Fuller, M. Wójcikowski, C. A. James, bjacob, dspoel, A. Fonari, petermr, orex, J. Janes, kebekus, D. Hall, J. Chen, C. Steinmann, P. Avery, H. D. Winter, K. Nishimra, and J.-N. Avila, "openbabel/openbabel: Open babel 3.1.0," Oct. 2016.

[34] J. Yang, C. Shen, and N. Huang, "Predicting or pretending: Artificial intelligence for protein-ligand interactions lack of sufficiently large and unbiased datasets," *Frontiers in Pharmacology*, vol. 11, 2020.

[35] M. Volkov, J.-A. Turk, N. Drizard, N. Martin, B. Hoffmann, Y. Gaston-Mathé, and D. Rognan, "On the frustration to predict binding affinities from protein–ligand structures with deep neural networks," *Journal of Medicinal Chemistry*, vol. 65, no. 11, pp. 7946–7958, 2022. PMID: 35608179.

[36] J. Scantlebury, N. Brown, F. Von Delft, and C. M. Deane, "Data set augmentation allows deep learning-based virtual screening to better generalize to unseen target classes and highlight important binding interactions," *Journal of Chemical Information and Modeling*, vol. 60, no. 8, pp. 3722–3730, 2020. PMID: 32701288.

[37] C. J. Radoux, T. S. Olsson, W. R. Pitt, C. R. Groom, and T. L. Blundell, "Identifying interactions that determine fragment binding at protein hotspots," *Journal of medicinal chemistry*, vol. 59, no. 9, pp. 4314–4325, 2016.

[38] R. Skyner and F. von Delft, "Xchem, fragalysis." `https://fragalysis.diamond.ac.uk/`. Accessed: 2022-07-30.

[39] C. Wang and Y. Zhang, "Improving scoring-docking-screening powers of protein–ligand scoring functions using random forest," *Journal of Computational Chemistry*, vol. 38, no. 3, pp. 169–177, 2017.

[40] J. Lu, X. Hou, C. Wang, and Y. Zhang, "Incorporating explicit water molecules and ligand conformation stability in machine-learning scoring functions," *Journal of Chemical Information and Modeling*, vol. 59, no. 11, pp. 4540–4549, 2019. PMID: 31638801.

[41] S. Salentin, S. Schreiber, V. J. Haupt, M. F. Adasme, and M. Schroeder, "PLIP: fully automated protein–ligand interaction profiler," *Nucleic Acids Research*, vol. 43, pp. W443–W447, 04 2015.

[42] `https://fragalysis.diamond.ac.uk/viewer/react/download/tag/5740113a-7603-4af4-9523-7f902186d4a2`. Accessed: 2022-10-14.

[43] A. Carbery, R. Skyner, F. von Delft, and C. M. Deane, "Fragment libraries designed to be functionally diverse recover protein binding information more efficiently than standard structurally diverse libraries," *Journal of Medicinal Chemistry*, vol. 65, no. 16, pp. 11404–11413, 2022. PMID: 35960886.

[44] M. Schuller, G. J. Correy, S. Gahbauer, D. Fearon, T. Wu, R. E. Díaz, I. D. Young, L. C. Martins, D. H. Smith, U. Schulze-Gahmen, T. W. Owens, I. Deshpande, G. E. Merz, A. C. Thwin, J. T. Biel, J. K. Peters, M. Moritz, N. Herrera, H. T. Kratochvil, A. Aimon, J. M. Bennett, J. B. Neto, A. E. Cohen, A. Dias, A. Douangamath, L. Dunnett, O. Fedorov, M. P. Ferla, M. R. Fuchs, T. J. Gorrie-Stone, J. M. Holton, M. G. Johnson, T. Krojer, G. Meigs, A. J. Powell, J. G. M. Rack, V. L. Rangel, S. Russi, R. E. Skyner, C. A. Smith, A. S. Soares, J. L. Wierman, K. Zhu, P. O'Brien, N. Jura, A. Ashworth, J. J. Irwin, M. C. Thompson, J. E. Gestwicki, F. von Delft, B. K. Shoichet, J. S. Fraser, and I. Ahel, "Fragment binding to the nsp3 macrodomain of sars-cov-2 identified through crystallographic screening and computational docking," *Science Advances*, vol. 7, no. 16, p. eabf8711, 2021.

[45] N. Imprachim, Y. Yosaatmadja, and J. A. Newman, "Crystal structures and fragment screening of sars-cov-2 nsp14 reveal details of exoribonuclease activation and mrna capping and provide starting points for antiviral drug development," *bioRxiv*, 2022.

[46] `https://fragalysis.diamond.ac.uk/viewer/react/download/tag/01f41754-b2bb-4817-acc3-a5ebe820316d`. Accessed: 2022-10-14.

[47] `https://fragalysis.diamond.ac.uk/viewer/react/download/tag/3df36d6b-3a5b-400d-97eb-af3b0e0df42d`. Accessed: 2022-10-14.